



Synthesize and characterization of Co-complex as interlayer for Schottky type photodiode

A. Kocyigit¹ · M. Yildirim² · D. A. Kose³ · D. E. Yildiz⁴

Received: 29 August 2021 / Revised: 27 October 2021 / Accepted: 4 December 2021 /
Published online: 20 January 2022

© The Author(s), under exclusive licence to Springer-Verlag GmbH Germany, part of Springer Nature 2021

Abstract

Nicotinamide/nicotinic acid complexes with centered Co metal (called Co-complexes) were synthesized by chemically reactions and characterized by thermogravimetric analysis (TGA), UV–Vis spectrometer and atomic force microscopy (AFM) techniques. While the composition of the Co-complexes was confirmed by TGA, the compatibilities of the Co-complexes for optoelectronic devices were revealed by UV–Vis spectrometer and AFM techniques. The Co-complexes were dissolved in water for various weight amounts of 0.5 mg, 1.0 mg, 2.0 mg and 3.0 mg, and solutions were coated onto Si wafer pieces to obtain Co-complex interlayered film in the Al/p-Si metal semiconductor devices. I – V and I – t measurements were performed to investigate photodiode and photodetector behaviors of the Al/Co-complex/p-Si devices for various light power illumination intensities. The result revealed that Al/Co-complex/p-Si devices can be used for optoelectronic applications.

Keywords Nicotinamide/nicotinic acid complexes · Al/p-Si · Metal semiconductor devices · Optoelectronic applications

Introduction

The complex compounds with transition metals attract attention due to their good properties for industrial applications in nanotechnology, sensor applications, magnets, optoelectronic materials, energy transmission and storage, gas storage,

✉ A. Kocyigit
kocyigita58@gmail.com

¹ Department of Electronics and Automation, Vocational High School, Bilecik Şeyh Edebali University, 11230 Bilecik, Turkey

² Department of Biotechnology, Faculty of Science, Selcuk University, 42030 Konya, Turkey

³ Department of Chemistry, Faculty of Arts and Sciences, Hitit University, 19030 Corum, Turkey

⁴ Department of Physics, Faculty of Arts and Sciences, Hitit University, 19030 Corum, Turkey

separation and catalysis [1–5]. Molecules are designed as donor ligands, usually over N or O atoms, forming a two-dimensional or three-dimensional mesh structure. These ligands are also positioned as bridges between metal centers for supporting the polymeric nature of the structures. In these structures, ligands such as salicylates, dicarboxylate succinate, maleate, terephthalate, polycarboxylate, coumarylate, 1,3,5-benzenetricarboxylate, 1,2,4,5-benzenetetracarboxylate, benzene-1,3,5-tricarboxylate, diphenate, etc., are frequently used as binders [6–12]. Such coordination compounds are also called metal–organic frameworks. Studies on metal–organic frameworks (MOFs) structures (syntheses, characterizations and applications) have increased with significant momentum in recent years [13–15]. Due to their large surface areas and porosity, they can find many usage areas, especially gas adsorption, separation and catalysis. Surface areas and pores can be easily changed by changing the organic binder [16–21]. The structural and chemical properties of coordination compounds containing various ligands may also change by that way [22–26].

Metal–semiconductor (MS) devices have great importance for electronic devices owing to their metallic and ohmic behaviors, and thus, they can be employed in diodes, transistors, capacitors, etc. [27–29]. The interlayer materials are so important for increasing effectiveness of MS devices because they can passivate dangling bonds, increase electron mobility after illumination, change barrier height between metal and semiconductor and decrease leakage current throughout MS devices [30]. The metal-complex structures can also be employed for MS devices as interfacial layer to improve electrical behaviors.

In this paper, we synthesized and characterized the complex compound with Co metals which were structurally derivative of each other, but obtained by the coordination of ligands: one of was coordination over the pyridine nitrogen (nicotinamide), and the other was over the carboxylate oxygen (nicotinic acid) to the Co(II) metal cation. The structural, optical and morphological properties of the Co-complex structures were investigated to illuminate compatibility for Schottky type photodiodes by various instruments for various complex amounts. The Al/Co-Complex/p-Si devices with various molarity were characterized by *I–V* measurements under various light power intensities.

Experimental details

Synthesis

Nicotinic acid ($C_6H_5NO_2$), nicotinamide ($C_6H_5N_2O$), sodium bicarbonate ($NaHCO_3$), cobalt acetate tetra hydrate ($Co(CH_3COO)_2 \cdot 4H_2O$) were purchased from the Sigma-Aldrich company and used in the synthesis of the complexes without further purification.

Firstly, to increase the solubility of the nicotinic acid molecule in water, it was converted into sodium salt according to Eq. 1 in Fig. 1. 0.02 mol (2.462 g) nicotinic acid was included into 50 mL of distilled water, and 0.02 mol $NaHCO_3$ (1.68 g) was slowly added to it as a solid to prevent foaming due to prevent overflow and the sudden release of CO_2 in the solution. Secondly, 0.02 mol (2.442 g) solution of

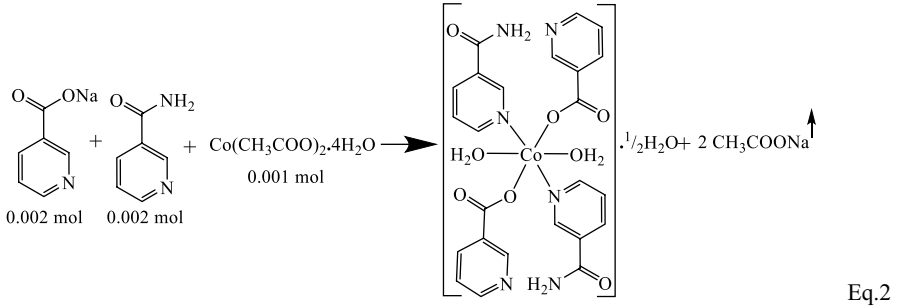
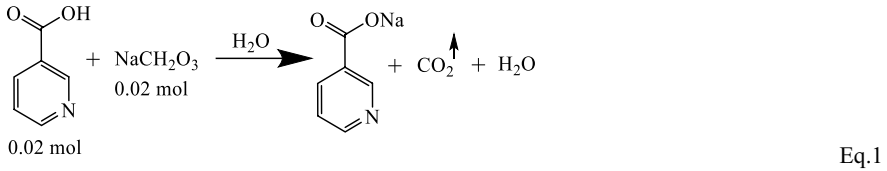


Fig. 1 Nicotinic acid/nicotinamide metal-complex synthesis

nicotinamide molecule for another neutral ligand prepared in 50 ml of purified water was added into the nicotinate ligand. The resulting solution was mixed in a magnetic stirrer for 30 min to obtain a homogenous solution. Finally, the acetate salt of the Co (II) cation for acting as the coordination center was slowly added to the reaction vessel as 0.01 mol (2.491 g) solid according to Eq. 2 in Fig. 1. The obtained solution was stirred on a magnetic stirrer hot-plate at 60 °C for 5 h. The diminished solvent of the solution was preserved by adding not more than 100 mL in total. There were two main purposes of mixing by heating. The first was to help the total solution to be allowed to crystallize at room temperature to react more easily at a temperature above room temperature. The other reason was to ensure that the reaction residue acetic acid (CH₃COOH), which had a very low pH increasing feature as a contaminant, was removed from the environment as much as possible [23, 31, 32]. The last solution was transferred into a beaker and sealed with paraffin and left to stand until crystal formed. The white acicular crystals formed after about 10–15 days were collected and stored for structural analysis.

Chemical composition analysis data for the synthesized complex compound confirmed the proposed molecular formula. While chemical composition data of complex experimentally were C: 47.84%, H: 3.85% and N: 14.13%, theoretically calculated chemical composition was C: 48.09%, H: 4.18% and N: 14.03%.

Device fabrications

A one-side polished p-type Si wafer was used as substrate and semiconductor material for the fabricating of the Schottky type photodiode. It had $7.3 \times 10^{15} \text{ cm}^{-3}$ carrier concentrations and (100) crystalline orientation according to the manufacturer. The wafer was sliced into $1 \times 2 \text{ cm}^2$ pieces and then cleaned by an ultrasonic cleaner in acetone, propanol and distilled water for 10 min in each solvent. Natural SiO₂ layers on the Si wafer pieces were removed by etching in the HF:H₂O (1:10) solution

for 30 s. Then, the pieces were immediately carried into a thermal evaporator, and Al metal was evaporated as 100-nm-thicknesses onto unpolished surfaces of the pieces. After, the pieces were annealed for only 5 min to obtain ohmic back contact in the N_2 filled oven. Then, the 0.5, 1.0, 2.0 and 3.0 mg $Co(C_6H_6N_2O)_2(C_6H_4NO_2)_2 \cdot \frac{1}{2}H_2O$ g complex was dissolved in four different vessels in 10 ml deionized water. Thus, 0.5 mg Co-complex, 1.0 mg Co-complex, 2.0 mg Co-complex and 3.0 mg Co-complex dissolved solution were applied onto polished side of Si surfaces by spin coating technique for 30 s at 3000 rpm, and the substrates were heated up on a heater at 80 °C for 1 h. The Co-complex/p-Si were transferred into thermal evaporator chamber to achieve Al metallic contacts on the top surfaces by a hole array mask with $7.85 \times 10^{-3} \text{ cm}^2$ area. Thus, 0.5, 1.0, 2.0 and 3.0 mg Co-complex dissolved solution were interlayered Al/p-Si devices to achieve various molarities of Co-complex material. The measurement system and schematic illustration of the Al/Co-Complex/p-Si devices have been shown in Fig. 2.

Characterization

The TGA analysis was performed by Shimadzu TG60H instrument. The UV–Vis spectrometer result was collected by Shimadzu UV-3600i Plus UV–Vis-NIR Spectrophotometer. The AFM images of the devices were taken by Park XE-100 AFM from Park Systems. I – V characteristics of the obtained photodiode were measured by Fytronix FY-7000 measurement system for dark and various light power illumination intensities.

Results and discussion

Structural properties

The thermal analysis curves of the coordination compound with mixed ligands of the cobalt metal cation containing nicotinic acid/nicotinamide ligands have been

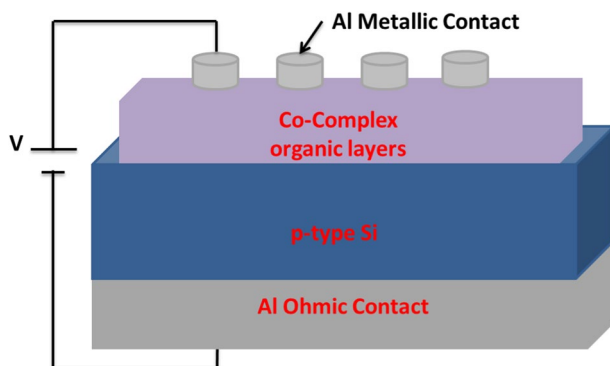


Fig. 2 Schematic illustration as well as measurement setup of the Al/Co-Complex/p-Si devices

presented in Fig. 3. The degradation steps and degradation products also have been shown in Table 1. It is seen that the thermal degradation of the complex containing the Co (II) metal cation centered on nicotinate-nicotinamide ligands that takes place in four steps. The first step is the dehydration step of the complex structure, and this step consists of the removal a total of seven aqua molecules, five located outside the coordination sphere and two in the coordinated position to the metal (exp. 18.83%, calc. 18.71%). This result can be attributed to the degradation of organic ligands in the second step and the removal of $-\text{NH}_2$ groups from the nicotinamide structures (exp. 4.59%, calc. 4.75%). The next step is the step where the amount of organic residue is burned away, and the weight loss is the highest. In this step, it is predicted that the pyridine ring of the nicotinamide ligand burns together with the remaining parts of nicotinamide ligands (exp. 53.87%, calc. 54.69%). In the fourth and last step, it is observed that the last organic derivatives remaining in the complex structure are burned, and the theoretical and experimental weight losses also support our claim (exp. 9.95%, calc. 10.69%). At the same time, the experimental and theoretical percent weight losses of the final decomposition product are in good agreement (exp. 12.76%, calc. 11.16%). The reason for the slightly higher experimental residue percentage was interpreted in the thermal analysis performed in an inert nitrogen atmosphere that the carbon residues in the structure could not be completely burned due to the lack of sufficient oxygen in the environment. It is believed that carbon residues, which cannot be fully combusted, are deposited as carbonized carbon on the metal oxide remaining as the final decomposition product in the reaction vessel. For that reason, it was determined that the color of the expected yellowish metal oxide was black.

Optical properties

The optical band gap behavior of the Co-complex structure was investigated by UV–Vis spectrometer by using of Tauc plot [33]. Figure 4 shows the Tauc plot of the Co-complex material. The Co-complex exhibited direct band gap transition, and the band gap value was determined as 3.82 eV according to Tauc plot. This band gap value is suitable for optoelectronic applications, and Co-complex can be employed for optoelectronic devices.

Fig. 3 TG-DTG and DTA curves of the $[\text{Co}(\text{C}_6\text{H}_6\text{N}_2\text{O})_2(\text{C}_6\text{H}_4\text{NO}_2)_2(\text{H}_2\text{O})_2] \cdot 1/2(\text{H}_2\text{O})$ complex

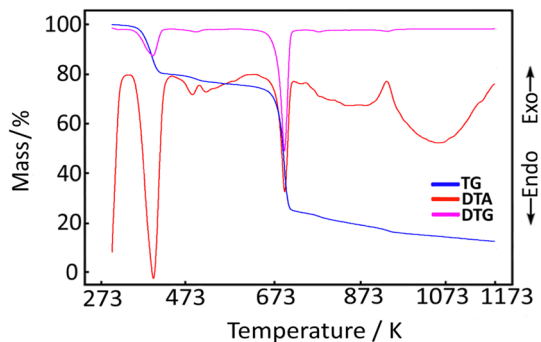


Table 1 Thermal analysis data of metal-nicotinate / nicotinamide mixed ligand complex

Complexes	Temp. range (°C)	DTA _{max} (°C)	Removed groups	Mass loss (%)		Remain product (%)		Decomp. product	Color
				Exp.	Calc.	Exp.	Calc.		
$[\text{Co}(\text{C}_6\text{H}_6\text{N}_2\text{O})_2(\text{C}_6\text{H}_4\text{NO}_2)_2(\text{H}_2\text{O})_2] \cdot 5\text{H}_2\text{O}$ $\text{C}_{24}\text{H}_{34}\text{CoN}_6\text{O}_{13}$ 673.50 g/mol	1	71–140	123	7 H ₂ O	18.83	18.71			white
	2	166–341	213;244	2 NH ₂	4.59	4.75			
	3	347–518	422	C ₆ H ₄ NO C ₅ H ₄ N	53.87	54.69			
	4	521–865	–591;772	CO; CO ₂	9.95	10.69	12.76	11.16	
									Black

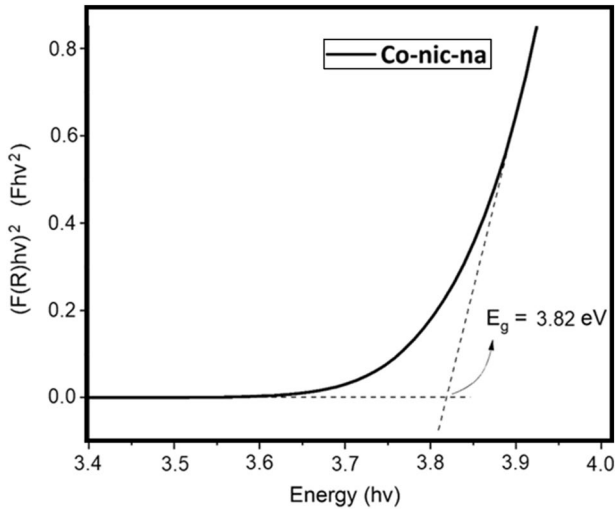


Fig. 4 Tauc plot of the $[\text{Co}(\text{C}_6\text{H}_6\text{N}_2\text{O})_2(\text{C}_6\text{H}_4\text{NO}_2)_2(\text{H}_2\text{O})_2] \cdot 1/2(\text{H}_2\text{O})$ complex

Morphological properties

AFM images of the Co-Complex interlayers have been shown in Fig. 5 for changing molarities in water solvent. While the Co-Complex molarity increased, the grain size of the Co-complex film increased and changed from the spherical shape to shapeless agglomeration structures. However, all the films exhibit a uniform surface, and they have a suitable surface for the metal semiconductor interfacial layer [34]. The thicknesses of the 0.5 mg Co-complex, 1.0 mg Co-complex, 2.0 mg Co-complex and 3.0 mg Co-complex were determined as 120 nm, 124 nm, 130 nm and 136 nm, respectively, by AFM.

Electrical properties

In I - V plots of the Al/Co-Complex/p-Si photodetector devices have been given in Fig. 6a–d for 0.5 mg, 1.0 mg, 2.0 mg and 3.0 mg Co-complex amounts dissolved same volume water, respectively, for increasing light power intensity from dark to 100 mW/cm^2 by 20 mW/cm^2 interval. There can be seen a shift toward forward bias region at minimum current values of the devices under light illumination while the Co-complex amount increases to 1.0 mg. This shift can be attributed to photovoltaic behavior of the Al/Co-Complex/p-Si devices. Furthermore, the devices showed good photodiode properties due to increasing current at reverse biases when the light power intensity increased [35]. The current values of the Al/Co-Complex/p-Si photodetector devices increased up to 2.0 mg Co-complex amount, and then slightly decreased for each light power intensity at reverse biases. The reason of this slightly decrease at the current values of 3.0 mg Co-complex used device can be attributed to increasing interface states as well as defects due to increasing of molarity [36, 37].

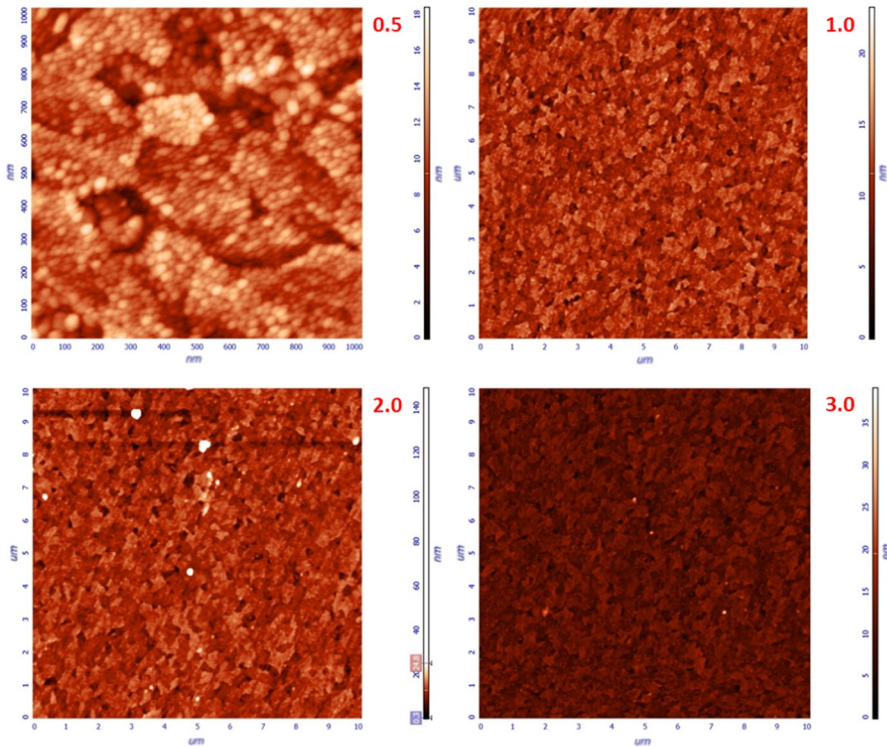


Fig. 5. 2D AFM images of the Co-Complex depending increasing dissolved materials

Figure 7a–d display the rectifying ratio (RR) versus power intensity plots of the Al/Co-Complex/p-Si photodetector devices for 0.5 mg, 1.0 mg, 2.0 mg and 3.0 mg Co-complex dissolved solution, respectively. All devices exhibited well rectifying behaviors owing to having low reverse bias and higher forward bias currents at the I – V characteristics under dark condition. Furthermore, the RR values decreased by increasing the Co-complex amount due to increasing reverse bias currents. The devices continued to protect their rectifying behaviors even if increasing light power intensity. The results highlight that Co-complex interlayer can be improve diode behavior of the Al/p-Si by increasing photocurrent at reverse biases.

The device parameters such as barrier height (Φ_b) and ideality factor (n) values can be calculated by thermionic emission theory, and their calculation formulas are given everywhere [38–40]. Figure 8a–d show barrier height and ideality factor changes for increasing light power intensity of the Al/Co-Complex/p-Si devices in the Co-complex amounts of 0.5 mg, 1.0 mg, 2.0 mg and 3.0 mg in solution, respectively. Generally, the Φ_b values increased suddenly for 20 mW/cm² light power intensity and then decreased for other light power intensities. These changes at the Φ_b values can be attributed increasing barrier inhomogeneity in the complex structures [41]. The ideality factor values decreased with increasing Co-complex amounts in the solution, but they increased with increasing light power intensity for all devices owing to increasing forward bias current velocity with the increasing

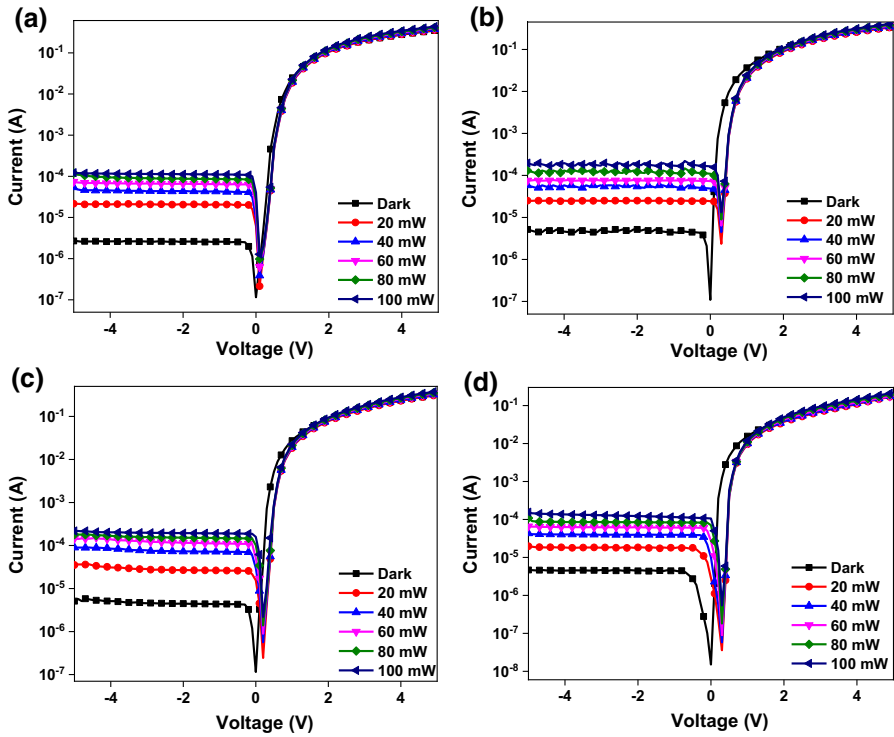


Fig. 6 In I – V plots of the various ratios of the Al/Co-Complex/p-Si devices **a** 0.5 mg, **b** 1.0 mg, **c** 2.0 mg and **d** 3.0 mg Co-complex dissolved solutions

light power. The higher values of the ideality factor than unity can be attributed to barrier inhomogeneity and interface states [42]. The calculated Φ_b and n values have been listed in Table 2 for the various Co-complex amounts in the solution. While the n values decreased with increasing Co-complex amount, the barrier height values exhibited fluctuation due to barrier inhomogeneity of the devices.

The junction resistance (R_j) provide to better understanding of the metal semiconductor devices and can be determined from I – V characteristics by the formalism of the $R_j = dV/dI$ [43]. It has shunt resistance (R_{sh}) and series resistance (R_s) components for the reverse and forward bias regions, respectively [44]. R_j – V plots of the Al/Co-Complex/p-Si devices have been displayed in Fig. 9a–d for the Co-complex amounts of 0.5 mg, 1.0 mg, 2.0 mg and 3.0 mg in same volume water solutions, respectively. The R_{sh} and R_s regions at reverse and forward biases have been clearly seen in the R_j – V plots. The devices exhibited high R_{sh} ($10^6 \Omega$ level) and low R_s ($10^1 \Omega$ level) values, and these values confirmed suitable device performance for optoelectronic applications [45].

Norde technique can also be used to calculate series resistance and to confirm the accuracy of the barrier height values of the metal semiconductor devices. Figure 10a–d indicate the Norde function plots of the Al/Co-Complex/p-Si devices

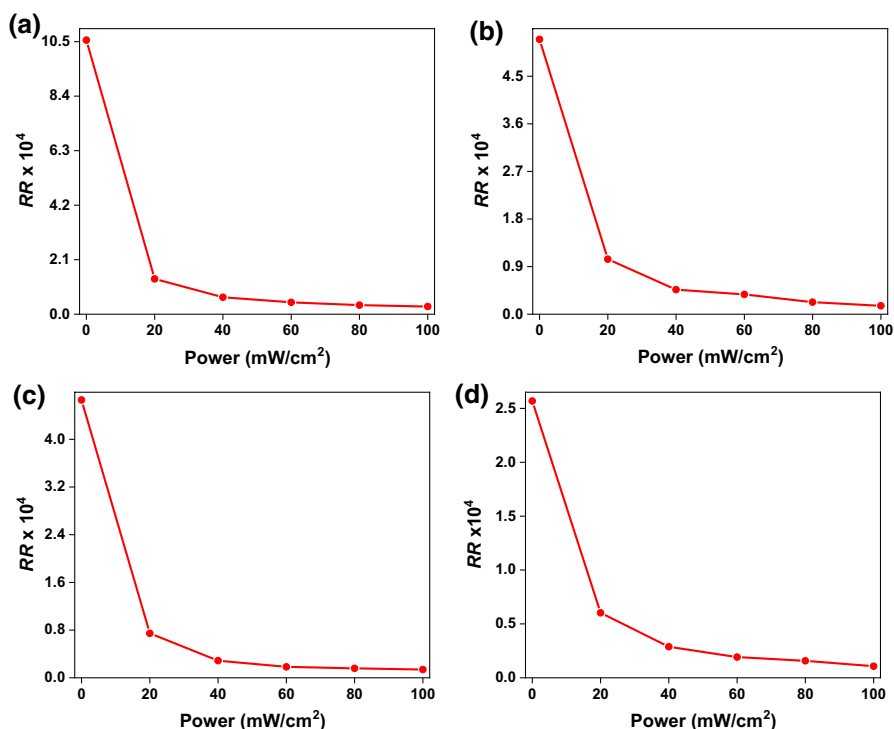


Fig. 7 RR versus power intensity plots of the various ratio of the Al/Co-Complex/p-Si devices **a** 0.5 mg, **b** 1.0 mg, **c** 2.0 mg and **d** 3.0 mg Co-complex dissolved solutions

for Co amount of 0.5 mg, 1.0 mg, 2.0 mg and 3.0 mg, respectively. The plots clearly show normal Norde function profiles depending on the voltage. The calculated Φ_b and R_s values have been listed in Table 2 for various amount Co-complex interlayered devices. The calculated Φ_b values are in good consistency with the Φ_b values calculated from thermionic emission theory. The R_s values also have good harmony with the R_s values obtained from the R_f - V plots of the devices. The small deviation can be attributed to approximation types as well as non-ideal device structures [46].

The Cheung method also can be used to calculate series resistance, ideality factor and barrier height values for metal semiconductor devices, and the calculation processes can be found everywhere [47, 48]. While the intercepts of the $dV/d(\ln I)$ and $H(I)$ Cheung functions are used to calculate ideality factor and barrier height, the slopes of these functions reveal two series resistance values [49]. If these series resistance values are close to each other, the Cheung method works right [50]. Figure 11a–d present the Cheung plots of the Al/Co-Complex/p-Si devices for Co-complex amounts of 0.5 mg, 1.0 mg, 2.0 mg and 3.0 mg in same volume water solvent, respectively. The plots of the $dV/d(\ln I)$ functions exhibited straight lines with some of deviation from linearity due to unwanted defects in

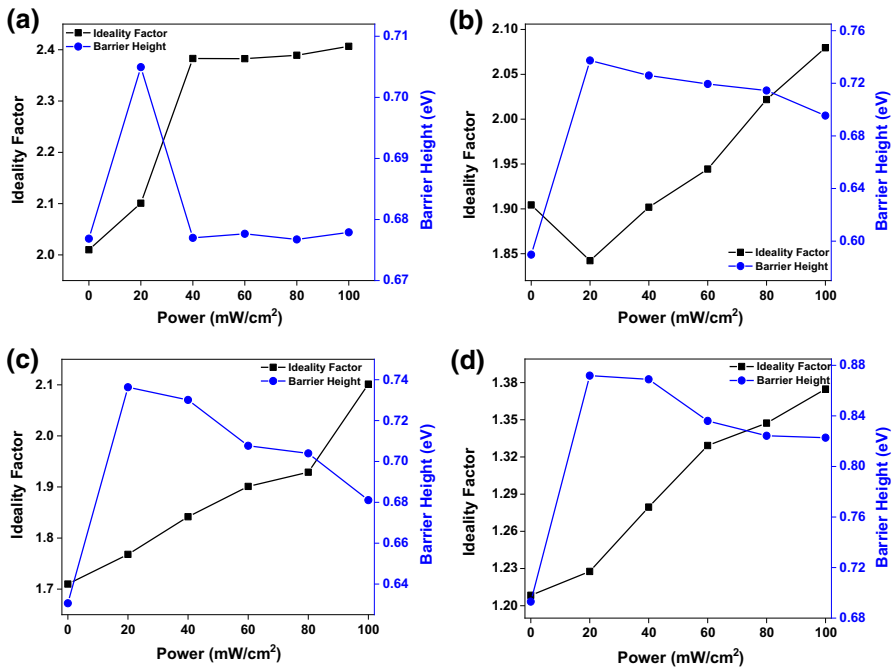


Fig. 8 $n-\Phi_b$ plots of the various Co doped Al/Co-Complex/p-Si devices **a** 0.5 mg, **b** 1.0 mg, **c** 2.0 mg and **d** 3.0 mg Co-complex dissolved solutions

the interface of the devices [51]. The calculated n , Φ_b and R_s values have been tabulated in Table 2 for Co-complex amounts in the same solutions of the Al/Co-Complex/p-Si devices. The obtained n , Φ_b and R_s values have good harmony with the device parameters obtained from other techniques, and the results confirm the consistency of the other techniques.

The current transient measurements in an applied voltage for photodiodes can provide to understand photosensitivity, responsivity as well as detectivity characteristics depending on the changing power intensity [52–55]. The current transient plots of the Al/Co-Complex/p-Si devices for Co-complex amounts of 0.5 mg, 1.0 mg, 2.0 mg and 3.0 mg in the same volume solution have been presented in Fig. 12a–d, respectively. The devices clearly gave immediate responses for every light power illumination. The obtained current amount decreased with the increasing Co-complex amount in the solvent for every light power.

Various detector parameters of the Al/Co-Complex/p-Si devices were calculated by using of the current transient measurements. The photocurrent (I_p), photosensitivity (K), responsivity (R) and specific detectivity (D^*) equations are addressed in the next equation, respectively.

$$I_p = I_{\text{light}} - I_{\text{dark}} \tag{1}$$

Table 2 The device parameters of the Al/Co-Complex/p-Si devices for various Co-complex amounts at dark $I-V$ measurements

Co-complex amounts (mg)	Saturation current (I_0)	n ($I-V$)	n cheung	$\Phi_b(I-V)$ (eV)	Φ_b cheung (eV)	Φ_b norde (eV)	R_s cheung ($\Omega(H(f))$)	R_s cheung ($(\Omega(d\ln(f)))$)	R_s norde (Ω)
0.5	9.86×10^{-8}	2.01	2.38	0.68	0.67	0.70	10.61	11.95	56.01
1.0	2.86×10^{-6}	1.90	2.11	0.59	0.63	0.62	12.12	12.66	18.99
2.0	5.90×10^{-7}	1.71	1.73	0.63	0.64	0.69	17.32	15.00	26.80
3.0	5.27×10^{-8}	1.21	1.32	0.69	0.68	0.64	37.01	41.82	57.35

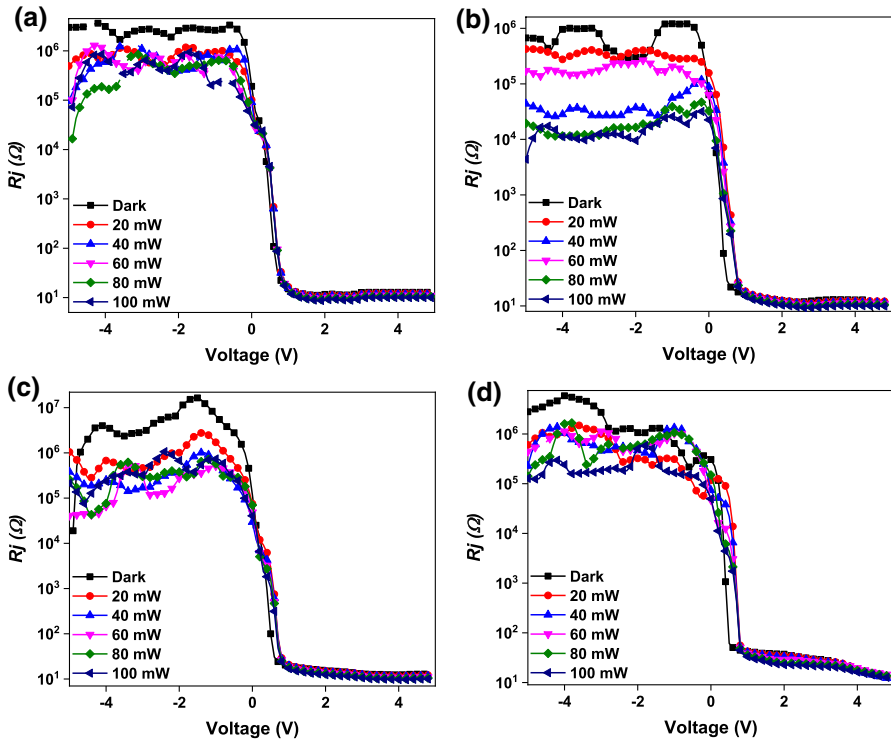


Fig. 9 R_f - V plots of the various Co doped Al/Co-Complex/p-Si devices **a** 0.5 mg, **b** 1.0 mg, **c** 2.0 mg and **d** 3.0 mg Co-complex dissolved solutions

$$K = \frac{I_p}{I_{\text{dark}}} \tag{2}$$

$$R = \frac{I_p}{PA} \tag{3}$$

$$D^* = R \sqrt{\frac{A}{2qI_{\text{dark}}}} \tag{4}$$

where A is the effective detector area, and P represents incident power density.

Table 3 exhibits changes of the I_p , R , K and D^* values depending on the increasing light power intensity for the 0.5 mg, 1.0 mg, 2.0 mg and 3.0 mg amounts of the Co-complex added solution of the Al/Co-Complex/p-Si devices. The I_p values slightly decreased with increasing Co-complex amount at lower light power, but they slightly increased toward higher light power intensity. This case can be attributed to that increasing molarity caused to increase interfacial traps to capture mobility charges more at lower light power. In the case of increasing light power intensity for every device, the I_p values increased almost linearly due to obtaining more

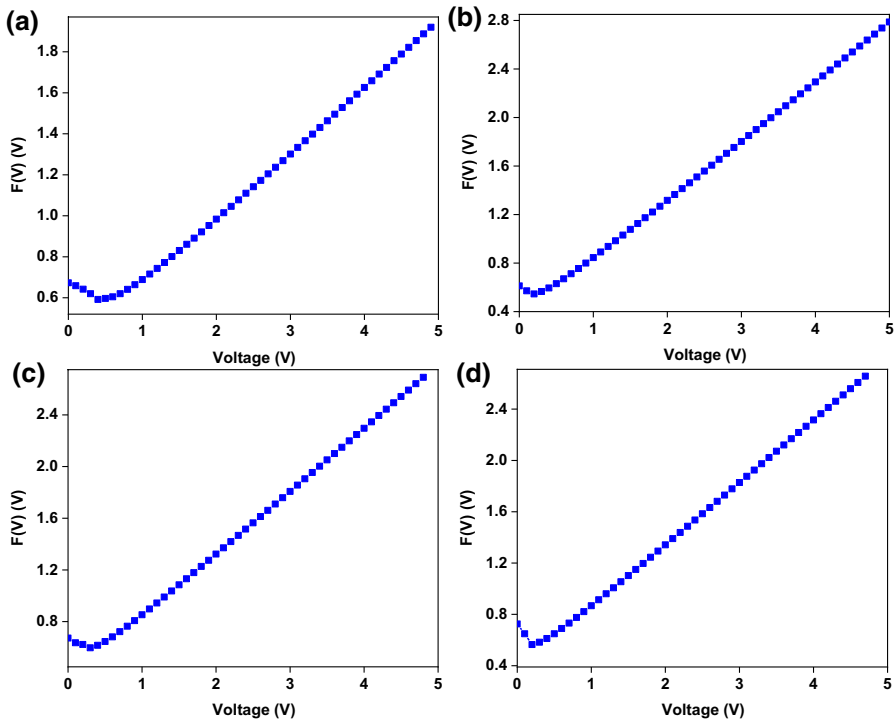


Fig. 10 $F(V) - V$ plots of the various Co doped Al/Co-Complex/p-Si devices **a** 0.5 mg, **b** 1.0 mg, **c** 2.0 mg and **d** 3.0 mg Co-complex dissolved solutions

charge carriers in the depletion regions of the devices. The K values increased both the increasing Co-complex amount in the Al/Co-Complex/p-Si devices and increasing light power intensity owing to linear relation of K and I_p . The increasing photosensitivity with increasing light power can be depended on the photoconductive behaviors of the Al/Co-Complex/p-Si devices [56]. The R values decreased with increasing light power depending on the reciprocal relation between the power and responsivity as well as increasing Co amount in the complex interlayer. While the Co-complex amount increased in the complex interlayer, D^* values increased. However, they generally decreased with increasing light power intensity.

Conclusion

Co metal centered Nicotinamide and nicotinic acid ligand complexes (Co-complexes) were synthesized, and characterized by TGA, UV-Vis spectroscopy and AFM. The TGA analysis revealed that the Co-complexes exhibited four degradation steps to confirm the composition of the Co-complex. UV-Vis spectroscopy was employed to show Tauc plot and determine the band gap of the Co-complex.

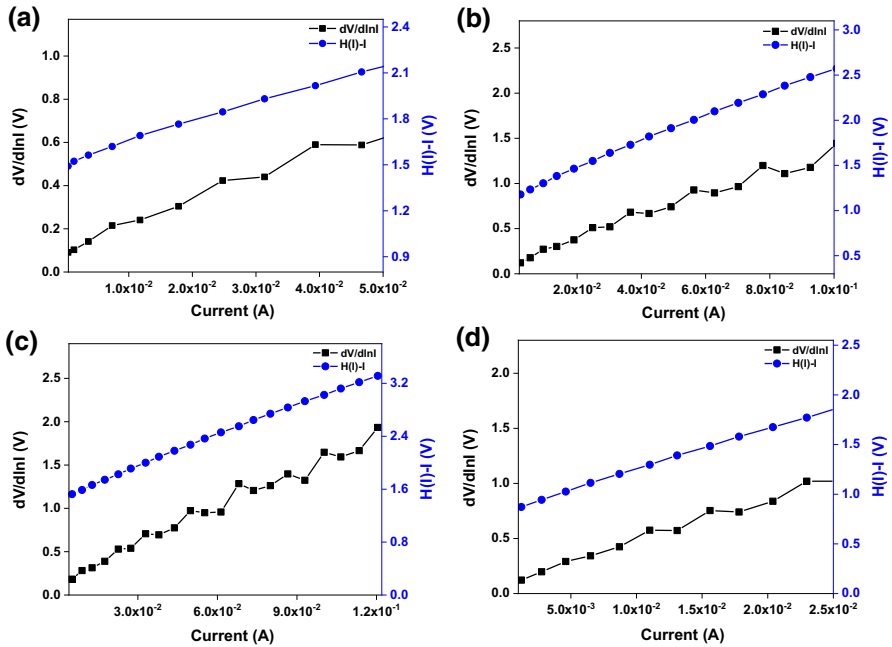


Fig. 11 Cheung plots of the various Co doped Al/Co-Complex/p-Si devices **a** 0.5 mg, **b** 1.0 mg, **c** 2.0 mg and **d** 3.0 mg Co-complex dissolved solutions

The Co-complex has 3.82 eV band gap energy value. The AFM images exhibited spherical shape with changing toward agglomeration by increasing molarity of the Co-complex. The Co-complexes with various weight amounts of 0.5 mg, 1.0 mg, 2.0 mg and 3.0 mg were dissolved in water, and then the solutions were coated onto Si wafer pieces to fabricate Al/Co-complex/p-Si devices. $I-V$ and $I-t$ measurements were employed to reveal electrical behaviors of the Co-complex in a metal semiconductor device for various light power illumination intensities. Various diode parameters such as ideality factor, barrier height, series resistance as well as rectifying ration values were calculated depending on the Co-complex molarity and light power illumination intensity. Furthermore, photodetector parameters also were calculated and discussed from $I-t$ characteristics of the Al/Co-complex/p-Si devices in details. The results indicate that complex materials can be employed for better photodiode and photodetector performances.

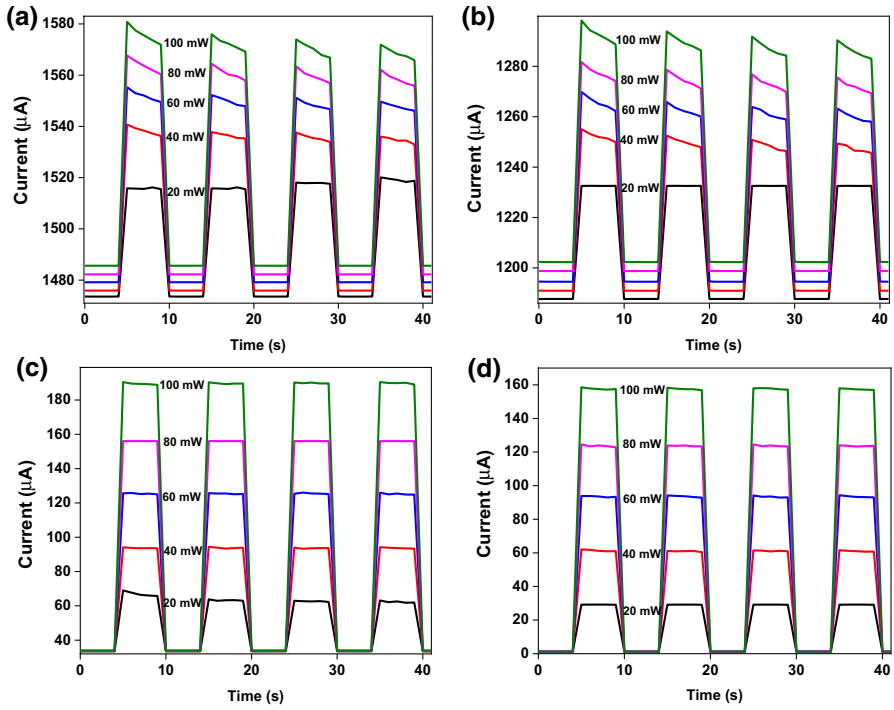


Fig. 12 $I-t$ plots of the various Co doped Al/Co-Complex/p-Si devices

Table 3 Various detector parameters of the Al/Co-Complex/p-Si devices for changing Co-complex amount

Co-complex amounts	Power (mW/cm ²)	Photocurrent (A)	Photosensitivity -	Responsivity (A/W)	Specific detectivity (Jones)
0.5 mg	20	5.00×10^{-5}	0.03	31.83	1.30×10^{11}
	40	6.00×10^{-5}	0.04	19.10	7.78×10^{10}
	60	8.00×10^{-5}	0.05	16.98	6.91×10^{10}
	80	9.00×10^{-5}	0.06	14.32	5.83×10^{10}
	100	9.00×10^{-5}	0.06	11.46	4.65×10^{10}
1.0 mg	20	4.49×10^{-5}	0.04	28.58	1.30×10^{11}
	40	6.41×10^{-5}	0.05	20.41	9.27×10^{10}
	60	7.53×10^{-5}	0.06	15.97	7.24×10^{10}
	80	8.29×10^{-5}	0.07	13.20	5.97×10^{10}
	100	9.58×10^{-5}	0.08	12.20	5.51×10^{10}
2.0 mg	20	3.55×10^{-5}	1.06	22.59	6.11×10^{11}
	40	6.05×10^{-5}	1.80	19.26	5.20×10^{11}
	60	9.19×10^{-5}	2.72	19.50	5.26×10^{11}
	80	1.22×10^{-4}	3.61	19.45	5.24×10^{11}
	100	1.56×10^{-4}	4.61	19.92	5.36×10^{11}
3.0 mg	20	2.81×10^{-5}	24.72	17.86	2.63×10^{12}
	40	6.01×10^{-5}	52.14	19.12	2.79×10^{12}
	60	9.24×10^{-5}	78.89	19.61	2.84×10^{12}
	80	1.23×10^{-4}	103.06	19.54	2.80×10^{12}
	100	1.56×10^{-4}	129.05	19.90	2.83×10^{12}

References

1. Yaghi OM, O'Keeffe M, Ockwig NW, Chae HK, Eddaoudi M, Kim J (2003) Reticular synthesis and the design of new materials. *Nature* 423:705–714. <https://doi.org/10.1038/nature01650>
2. Hagrman PJ, Hagrman D, Zubieta J (1999) Organic-inorganic hybrid materials: from “simple” coordination polymers to organodiamine-templated molybdenum oxides. *Angew Chem Int Ed* 38:2638–2684. [https://doi.org/10.1002/\(sici\)1521-3773\(19990917\)38:18%3c2638::aid-anie2638%3e3.3.co;2-w](https://doi.org/10.1002/(sici)1521-3773(19990917)38:18%3c2638::aid-anie2638%3e3.3.co;2-w)
3. Erxleben A (2003) Structures and properties of Zn(II) coordination polymers. *Coord Chem Rev* 246:203–228. [https://doi.org/10.1016/S0010-8545\(03\)00117-6](https://doi.org/10.1016/S0010-8545(03)00117-6)
4. Rao CNR, Natarajan S, Vaidhyanathan R (2004) Metal carboxylates with open architectures. *Angew Chem - Int Ed* 43:1466–1496. <https://doi.org/10.1002/anie.200300588>
5. Kim J, Lee U, Koo BK (2010) 1D chain crystal structure of copper(II) oxalate containing a 4,4'-bipyridine and 1,10-phenanthroline ligands: [Cu₂(ox)(4,4'-bpy)(phen)₂](NO₃)₂. *Bull Korean Chem Soc* 31:487–490. <https://doi.org/10.5012/bkcs.2010.31.02.487>
6. Kim J, Lee U, Koo BK (2010) Synthesis and 1D Chain crystal structure of zinc(II) terephthalate complex: [Zn(tp)(py)(H₂O)]_n. *Bull Korean Chem Soc* 31:1743–1746. <https://doi.org/10.5012/bkcs.2010.31.6.1743>
7. Koo BK, Kim J, Lee U (2010) Synthesis and crystal structures of di- and tetra-nuclear dicarboxylate-bridged copper(II) complexes. *Inorg Chim Acta* 363:1760–1766. <https://doi.org/10.1016/j.ica.2010.02.032>
8. Go YB, Wang X, Anokhina EV, Jacobson AJ (2005) Influence of the reaction temperature and pH on the coordination modes of the 1,4-Benzenedicarboxylate (BDC) ligand: a case study of the

- NiII(BDC)/2,2'-bipyridine system. *Inorg Chem* 44:8265–8271. <https://doi.org/10.1021/IC050644D>
9. Xu H, Wang R, Li Y (2004) Zn₂Na₂(BDC)₃-(DMF)₂-(μ-H₂O)₂: rare 3D channel-structures with pendant DMF constructed by carboxyl group bridging heterometallic ions. *J Mol Struct* 688:1–3. <https://doi.org/10.1016/J.MOLSTRUC.2003.07.003>
 10. Hao N, Li Y, Wang E, Shen E, Hu C, Xu L (2004) Hydrothermal synthesis and crystal structure of an infinite 1D ladderlike metal-organic compound: [Cu₂(btec)(2,2'-bipy)₂]_∞ (btec = 1,2,4,5-benzenetetracarboxylate). *J Mol Struct* 697:1–8. [https://doi.org/10.1016/S0022-2860\(03\)00349-1](https://doi.org/10.1016/S0022-2860(03)00349-1)
 11. Koo BK (2012) Synthesis and crystal structures of MN(II)- and NI(II)-dicarboxylate complexes with 1,10-phenanthroline. *Bull Korean Chem Soc* 33:2299–2304. <https://doi.org/10.5012/bkcs.2012.33.7.2299>
 12. Yaghi OM, Li H, Davis C, Richardson D, Groy TL (1998) Synthetic strategies, structure patterns, and emerging properties in the chemistry of modular porous solids. *Acc Chem Res* 31:474–484. <https://doi.org/10.1021/ar970151f>
 13. Zhang Z, Zhao Y, Gong Q, Lib Z, Li J (2013) MOFs for CO₂ capture and separation from flue gas mixtures: the effect of multifunctional sites on their adsorption capacity and selectivity. *Chem Commun* 49:653–661. <https://doi.org/10.1039/c2cc35561b>
 14. Baumann AE, Burns DA, Liu B, Thoi VS (2019) Metal-organic framework functionalization and design strategies for advanced electrochemical energy storage devices. *Commun Chem* 2:1–14. <https://doi.org/10.1038/s42004-019-0184-6>
 15. García-Valdivia AA, Pérez-Yáñez S, García JA, Fernández B, Cepeda J, Rodríguez-Diéguez A (2020) Magnetic and photoluminescent sensors based on metal-organic frameworks built up from 2-aminoisonicotinate. *Sci Rep* 10:1–17. <https://doi.org/10.1038/s41598-020-65687-6>
 16. Chae HK, Kim J, Friedrichs OD, O'Keeffe M, Yaghi OM (2003) Design of frameworks with mixed triangular and octahedral building blocks exemplified by the structure of [Zn₄O(TCA)₂] having the pyrite topology. *Angew Chem Int Ed* 42:3907–3909. <https://doi.org/10.1002/anie.200351546>
 17. Zhou HC, Long JR, Yaghi OM (2012) Introduction to metal-organic frameworks. *Chem Rev* 112:673–674. <https://doi.org/10.1021/cr300014x>
 18. Mueller U, Schubert M, Teich F, Puetter H, Schierle-Arndt K, Pastré J (2006) Metal-organic frameworks—prospective industrial applications. *J Mater Chem* 16:626–636. <https://doi.org/10.1039/b511962f>
 19. Jacoby M (2008) Heading to market with MOFS. *Chem Eng News* 86:13–16. <https://doi.org/10.1021/cen-v086n034.p013>
 20. Eddaoudi M, Kim J, Rosi N, Vodak D, Wachter J, O'Keeffe M, Yaghi OM (2002) Systematic design of pore size and functionality in isorecticular MOFs and their application in methane storage. *Science* 295:469–472. <https://doi.org/10.1126/science.1067208>
 21. Wang Z, Cohen SM (2007) Postsynthetic covalent modification of a neutral metal-organic framework. *J Am Chem Soc* 129:12368–12369. <https://doi.org/10.1021/ja074366o>
 22. Köse DA, Öztürk B, Şahin O, Büyükgüngör O (2013) Mixed ligand complexes of coumarilic acid/nicotinamide with transition metal complexes. *J Therm Anal Calorim* 115:1515–1524. <https://doi.org/10.1007/S10973-013-3415-6>
 23. Köse DA, Akkurt F, Şahin O, Büyükgüngör O (2014) Synthesis and structural characterization of a binuclear mixed-ligand (Salicylate and N, N-diethylnicotinamide) nickel(II) complex, its magnetic properties. [Ni₂(μ-Sal)₄(Dena)₂]H₂O. *J Chin Chem Soc* 61:1326–1332. <https://doi.org/10.1002/jccs.201400292>
 24. Köse DA, Necefoglu H, Icbudak H (2008) Synthesis and characterization of N, N-diethylnicotinamide-acetylsalicylate complexes of Co(II), Ni(II), Cu(II), and Zn(II). *J Coord Chem* 61:3508–3515. <https://doi.org/10.1080/00958970802074555>
 25. Köse DA, Ay AN, Şahin O, Büyükgüngör O (2012) A mononuclear, mixed (salicylate) (nicotinamide) complex of Zn(II) with penta- and hexa-coordination sites: a novel framework structure. *J Iran Chem Soc* 9:591–597. <https://doi.org/10.1007/S13738-012-0072-9>
 26. Icbudak H, Heren Z, Kose DA, Necefoglu H (2004) bis(nicotinamide) and bis(N, N-diethyl nicotinamide) *p*-hydroxybenzoate complexes of Ni(II), Cu(II) AND Zn(II). *J Therm Anal Calorim* 76:837–851. <https://doi.org/10.1023/B:JTAN.0000032269.12381.42>
 27. Kasper M, Gramse G, Hoffmann J, Gaquiere C, Feger R, Stelzer A, Smoliner J, Kienberger F (2014) Metal-oxide-semiconductor capacitors and Schottky diodes studied with scanning microwave microscopy at 18GHz. *J Appl Phys* 116:184301. <https://doi.org/10.1063/1.4897922>

28. Tian H, Tan Z, Wu C, Wang X, Mohammad MA, Xie D, Yang Y, Wang J, Li LJ, Xu J, Ren TL (2014) Novel field-effect schottky barrier transistors based on graphene-MoS₂ heterojunctions. *Sci Rep* 4:1–9. <https://doi.org/10.1038/srep05951>
29. Mathew M, Rout CS (2021) Schottky diodes based on 2D materials for environmental gas monitoring: a review on emerging trends, recent developments and future perspectives. *J Mater Chem C* 9:395–416. <https://doi.org/10.1039/d0tc04840b>
30. Çetinkaya HG, Alialy S, Altındal Ş, Kaya A, Uslu I (2015) Investigation of negative dielectric constant in Au/1 % graphene (GP) doped-Ca_{1.9}Pr_{0.1}Co₄Ox/n-Si structures at forward biases using impedance spectroscopy analysis. *J Mater Sci Mater Electron* 26:3186–3195. <https://doi.org/10.1007/s10854-015-2816-7>
31. Köse DA, Necefoğlu H, Şahin O, Büyükgüngör O (2012) Synthesis, structural, spectroscopic characterization, and structural comparison of 3-hydroxybenzoate and nicotinamide/*N*, *N*-diethylnicotinamide mixed ligand complexes with Zn(II). *J Therm Anal Calorim* 110:1233–1241. <https://doi.org/10.1007/s10973-011-2134-0>
32. Dağlı Ö, Köse DA, Şahin O, Şahin ZS (2017) The synthesis and structural characterization of coumarilic acid. *J Therm Anal Calorim* 128:1373–1383. <https://doi.org/10.1007/s10973-016-6053-y>
33. Jubu PR, Yam FK, Igba VM, Beh KP (2020) Tauc-plot scale and extrapolation effect on bandgap estimation from UV–Vis–NIR data—a case study of β-Ga₂O₃. *J Solid State Chem* 290:121576. <https://doi.org/10.1016/j.jssc.2020.121576>
34. Cifci OS, Bakir M, Meyer JL, Kocuyigit A (2018) Morphological and electrical properties of ATSP/p-Si photodiode. *Mater Sci Semicond Process* 74:175–182. <https://doi.org/10.1016/j.mssp.2017.10.039>
35. Gozeh BA, Karabulut A, Ismael CB, Saleh SI, Yakuphanoglu F (2021) Zn-doped CdO effects on the optical, electrical and photoresponse properties of heterojunctions-based photodiodes. *J Alloys Compd* 872:159624. <https://doi.org/10.1016/j.jallcom.2021.159624>
36. Altındal Ş, Karadeniz S, Tuğluoğlu N, Tataroglu A (2003) The role of interface states and series resistance on the *I*–*V* and *C*–*V* characteristics in Al/SnO₂/p-Si Schottky diodes. *Solid State Electron* 47:1847–1854. [https://doi.org/10.1016/S0038-1101\(03\)00182-5](https://doi.org/10.1016/S0038-1101(03)00182-5)
37. Uslu H, Altındal Ş, Dökme I (2010) Illumination effect on electrical characteristics of organic-based Schottky barrier diodes. *J Appl Phys* 108:104501. <https://doi.org/10.1063/1.3504598>
38. Peta KR, Kim MD (2018) Leakage current transport mechanism under reverse bias in Au/Ni/GaN Schottky barrier diode. *Superlattices Microstruct* 113:678–683. <https://doi.org/10.1016/j.spmi.2017.11.056>
39. Yıldız DE (2018) Electrical properties of Au–Cu/ZnO/p-Si diode fabricated by atomic layer deposition. *J Mater Sci Mater Electron* 29:17802–17808. <https://doi.org/10.1007/s10854-018-9889-z>
40. Yigiterol F, Güllü HH, Yıldız Bayraklı D.E. (2018) Temperature-dependent electrical characteristics of Au/Si₃N₄/4H-n-SiC MIS diode. *J Electron Mater* 47:2979–2987. <https://doi.org/10.1007/s11664-018-6155-3>
41. Orak İ, Kocuyigit A, Karataş Ş (2018) The analysis of the electrical and photovoltaic properties of Cr/p-Si structures using current-voltage measurements. *Silicon* 10:2109–2116. <https://doi.org/10.1007/s12633-017-9731-x>
42. Balbasi CD, Terlemezoğlu M, Gullu HH, Yıldız DE, Parlak M (2020) Electrical characterization of CdZnTe/Si diode structure. *Appl Phys A Mater Sci Process* 126:614. <https://doi.org/10.1007/s00339-020-03772-3>
43. Rao LD, Reddy VR, (2016) Electrical parameters and series resistance analysis of Au/Y/p-InP/Pt Schottky barrier diode at room temperature. In: AIP Conference Proceedings, AIP Publishing LLC, Melville, p 120020
44. Kocuyigit A, Yilmaz M, Aydoğan S, İncekara Ü, Kacıs H (2021) Comparison of n and p type Si-based Schottky photodiode with interlayered Congo red dye. *Mater Sci Semicond Process* 135:106045. <https://doi.org/10.1016/j.mssp.2021.106045>
45. Taşçıoğlu İ, Farooq WA, Turan R, Altındal Ş, Yakuphanoglu F (2014) Charge transport mechanisms and density of interface traps in MnZnO/p-Si diodes. *J Alloys Compd* 590:157–161. <https://doi.org/10.1016/J.JALLCOM.2013.12.043>
46. Yıldırım M, Kocuyigit A, Sarılmaz A, Ozel F (2019) The effect of the triangular and spherical shaped CuSbS₂ structure on the electrical properties of Au/CuSbS₂/p-Si photodiode. *J Mater Sci Mater Electron* 30:332–339. <https://doi.org/10.1007/s10854-018-0297-1>

47. Anh Tuan TT, Kuo D-H (2015) Characteristics of RF reactive sputter-deposited Pt/SiO₂/n-InGaN MOS Schottky diodes. *Mater Sci Semicond Process* 30:314–320. <https://doi.org/10.1016/j.mssp.2014.10.021>
48. Yilmaz M, Kocyigit A, Cirak BB, Kacus H, Incekara U, Aydogan S (2020) The comparison of Co/hematoxylin/n-Si and Co/hematoxylin/p-Si devices as rectifier for a wide range temperature. *Mater Sci Semicond Process* 113:105039. <https://doi.org/10.1016/j.mssp.2020.105039>
49. Cheung SK, Cheung NW (1986) Extraction of Schottky diode parameters from forward current-voltage characteristics. *Appl Phys Lett* 49:85. <https://doi.org/10.1063/1.97359>
50. Kocyigit A, Orak I, Çaldıran Z, Turut A (2017) Current–voltage characteristics of Au/ZnO/n-Si device in a wide range temperature. *J Mater Sci Mater Electron* 28:17177–17184. <https://doi.org/10.1007/s10854-017-7646-3>
51. Kocyigit A, Yilmaz M, Aydoğan Ş, Incekara Ü (2019) The effect of measurements and layer coating homogeneity of AB on the Al/AB/p-Si devices. *J Alloys Compd* 790:388–396. <https://doi.org/10.1016/j.jallcom.2019.03.179>
52. Shkir M, Khan MT, Ashraf IM, Almohammed A, Dieguez E, AlFaify S (2019) High-performance visible light photodetectors based on inorganic CZT and InCZT single crystals. *Sci Rep* 9:1–9. <https://doi.org/10.1038/s41598-019-48621-3>
53. Li C, Li J, Li Z, Zhang H, Dang Y, Kong F (2021) High-performance photodetectors based on nanostructured perovskites. *Nanomaterials* 11:1038. <https://doi.org/10.3390/nano11041038>
54. Gullu HH, Yildiz DE, Kocyigit A, Yıldırım M (2020) Electrical properties of Al/PCBM:ZnO/p-Si heterojunction for photodiode application. *J Alloys Compd* 827:154279. <https://doi.org/10.1016/j.jallcom.2020.154279>
55. Yildiz DE, Gullu HH, Sarilmaz A, Ozel F, Kocyigit A, Yıldırım M (2020) Dark and illuminated electrical characteristics of Si-based photodiode interlayered with CuCo₅S₈ nanocrystals. *J Mater Sci Mater Electron* 31:935–948. <https://doi.org/10.1007/s10854-019-02603-3>
56. Çavaş M, Yakuphanoglu F, Kaya S (2016) Electrical and photoconductivity properties of Al/CdFe₂O₄/p-Si/Al photodiode. *J Photon* 2016:1–7. <https://doi.org/10.1155/2016/4739020>

Publisher's Note Springer Nature remains neutral with regard to jurisdictional claims in published maps and institutional affiliations.